2016

Astrocyte Morphology and Cell Number in Rett Syndrome

Kenneth Taylor Holt
University of Alabama at Birmingham

ASTROCYTE MORPHOLOGY AND CELL NUMBER IN RETT SYNDROME

by

KENNETH TAYLOR HOLT

MICHELLE OLSEN, COMMITTEE CHAIR
VLADIMIR PARPURA
VITHAL K. GHANTA

A THESIS
Submitted to the graduate faculty of The University of Alabama at Birmingham,
In partial fulfillment of the requirements for the degree of
Master of Science
BIRMINGHAM, ALABAMA

2016

ASTROCYTE MORPHOLOGY AND CELL NUMBER IN RETT SYNDROME

KENNETH TAYLOR HOLT

DEPARTMENT OF BIOLOGY

ABSTRACT

Rett Syndrome (RTT) is an X-linked neurodevelopmental disorder caused by a mutation in the transcriptional regulator methyl CPG binding protein 2 (MECP2) gene that affects 1 in 10,000 female live births annually. RTT patients experience seemingly normal development for the first 12-18 months of life; this period of normal development is followed by developmental regression. The symptoms of Rett syndrome include severe cognitive deficits, seizures, loss of ambulation and gross motor skills, breathing abnormalities, hand stereotopies and gastrointestinal dysmotility. The basic science research for this disorder has focused almost exclusively on neuronal mechanisms, leaving limited understating of the role of other cell types. In this study, we examined the state of other cell types in this disease, specifically astrocytes. Examination of astrocyte morphology in the hippocampus revealed no difference in complexity when assessed with Sholl analysis. We further investigated astrocyte cell numbers in two regions of the brain, hippocampus and the motor cortex. Following analysis we discovered a trending decrease in the astrocyte to neuron ratio ($p = 0.0512$) in the hippocampus and a trending increase in astrocyte to neuron ratio ($p = 0.0669$) in the motor cortex. Our results suggest that astrocyte cell numbers, specifically astrocyte to neuron ratios, might be altered in the disease and could prove as an interesting new avenue of study for the disease.

DEDICATION

To Mom for always supporting me to follow my dreams and ambitions;

To Dad for teaching me to always keep those ambitions ever expanding;

To Erin for your amazing support, patience, & understanding along this journey.

ACKNOWLEDGMENTS

I would like to thank all of the graduate students and faculty who have made this thesis possible.

Foremost, I would like to express my utmost gratitude to my mentor Dr. Michelle Olsen. Without her continued support, guidance, teaching, and encouragement this work would not have been possible.

I would also like to thank my thesis committee, Dr. Vladimir Parpura and Dr. Vithal Ghanta for their time and guidance in the process.

TABLE OF CONTENTS

LIST OF FIGURES

INTRODUCTION

Rett syndrome (RTT) is a X-linked neurodevelopmental disorder caused by mutations in the transcriptional regulator *methyl CpG binding protein 2 (MECP2)* gene that affects 1 in 10,000 female live births annually (Laurvick et al., 2006). RTT patients experience seemingly normal development for the first 12-18 months of life; this period of normal development is followed by developmental regression. The symptoms of Rett syndrome include severe cognitive deficits, seizures, loss of ambulation and gross motor skills, breathing abnormalities, hand stereotopies and gastrointestinal dysmotility (Hagberg, Aicardi, Dias, & Ramos, 1983; Neul et al., 2010). No effective treatment strategies currently exist for those with Rett syndrome. The basic science research for this disorder has focused almost exclusively on neuronal mechanisms, leaving limited understading of the role of other cell types.

Methyl-CpG binding protein 2 (MeCP2) is a gene found on chromosome Xq28 that encodes for methyl-CpG binding protein 2. Previous research indicated that MeCP2 was only a transcriptional regulator that represses gene transcription, however, MeCP2's role in gene activation was recently demonstrated, when it was discovered that MeCP2 binds to lowly methylated promoter regions of highly transcribed genes (Chahrour et al., 2008). Specifically in the central nervous system, MeCP2 regulates the expression of a

variety of genes, including those involved in cell adhesion, the mitochondrial respiratory chain, neural differentiation and neural plasticity (Zachariah & Rastegar, 2012).

In 1999 it was discovered that mutations in MeCP2 are causative of Rett syndrome; since that time, interest has grown in the study of MeCP2 (Amir et al., 1999). According to the US Natural History study, 96% of individuals whom are diagnosed with Rett Syndrome are identified as having a MeCP2 mutation (Neul et al., 2008). These mutations have been noted with upwards of 200 unique sequence changes. According to the study 80% of the mutations were missense, nonsense, deletions and insertions, while the remaining 20% represent mutations that occur in one individual or within a small number of individuals. Notable differences in severity among the 80% of common mutations suggest a phenotype-genotype correlation (Neul et al., 2008; Cuddapah et al., 2014). While it has been found that the cause of Rett syndrome is a mutation in the *Mecp2* gene, a mutation in and of itself is not synonymous with the diagnosis of Rett syndrome. Some individuals with mutations of MeCP2 do not always have the features of Rett syndrome, while 4% have the criteria of Rett syndrome, without having the mutation (Cuddapah et al. 2015).

Mecp2 protein is ubiquitously expressed throughout the body, although its expression is highest in the brain and RTT is considered a neurological disease. Autopsy examination of brains obtained from RTT patients revealed a set of distinct changes in gross anatomy and cellular morphology (Armstrong, 2005). Specifically in the cerebral cortex, hypothalamus, and hippocampus a decrease in brain and neuronal size coupled with an increased packing density was seen (Bauman, Kemper et al. 1995, Bauman, Kemper et al. 1995). The hippocampus is located in the medial temporal lobe and is

associated with memory, emotion and spatial (Barr, Kiernan. 1993) In Rett syndrome specifically, changes in neuronal hyper excitability, robust changes in synaptic signaling, and deficits in short and long term synaptic plasticity, which are the molecular correlates of memory, have been detected (Dani, Chang et al. 2005, Zhang, He et al. 2008). More importantly, and relevant for the current study, ablation of MeCP2 from juvenile and adult mice resulted in hippocampal astrocytes with a significantly reduced complex morphology (Nguyen, Du et al. 2012).

A study investigating olfactory bulb biopsies reported a decrease in terminally differentiated olfactory receptor neurons, as well as a significant increase in the number of immature neurons in RTT individuals (Ronnett, Leopold et al. 2003). Pyramidal neurons from the frontal and motor cortex also showed a decrease in size and complexity of dendritic trees (Armstrong, Dunn et al. 1995, Armstrong, Dunn et al. 1998). Similar changes in neuronal morphology are recapitulated in murine models of the disease, specifically in the hippocampal CA1 region. These changes include smaller neurons, decreased dendritic branching, lower spine densities, dendritic swelling, and reduced diameter of dendritic spine heads (Purpura 1974, Belichenko, Wright et al. 2009). It is important to note the neuronal migration appeared to be normal and there is no evidence of neuronal atrophy, degeneration, or death. There were critical factors in differentiating RTT from a neurodegenerative disease (Jellinger, Armstrong, Zoghbi, & Percy, 1988). Furthermore, changes in myelination or glial reactivity are not observed in the RTT. All of these findings together suggested disrupted neuronal development, and until recently led to the nearly exclusive study of neurons in this disease.

Recent work by several groups suggests that another central nervous system cell type, the astrocyte, may also contribute to the etiology of Rett syndrome (Lioy, Garg et al. 2011). Astrocytes are the most abundant cell type in the CNS and carry out many functions that are essential for normal brain function. In the last several decades we have learned that astrocytes in the mature brain not only provide structural support, but are also key to maintaining the CNS microenvironment. Specifically by the buffering of K+ and neurotransmitters, they synthesize glutamine, which is shuttled to neurons and required for the synthesis of neuronal glutamate and GABA. Astrocytes integrate signals from neurons to regulate blood flow, they help to maintain the blood brain barrier, and serve as a scaffold for neuron guidance and contribute to synaptogenesis (Sofroniew & Vinters, 2010).

Astrocytes derive from neural precursor cells late in embryonic development (Hatada et al., 2008), however, the largest increase in astrocyte cell number occurs during the second and third post-natal weeks in the rodent (Bandeira, Lent, & Herculano-Houzel, 2009) when astrocyte cell numbers increase by as much as 90% across brain structures. During this same developmental time period astrocyte morphology changes robustly, demonstrating an increased complexity as astrocytes develop a dense network of fine processes (Bushong, Martone, & Ellisman, 2004).

Mature astrocytes have extremely complex morphologies, which have only recently been appreciated by technological advances which allow for confocal imaging of individually labeled cells such as dialistic labeling (Freeman, 2010; Oberheim, Wang, Goldman, & Nedergaard, 2006; Bushong et al., 2004). Primary branches extended from the soma divide into even finer processes to create a compact network of delicate

terminal processes (Bushong, Martone et al. 2004, Oberheim, Wang et al. 2006, Lovatt, Sonnewald et al. 2007, Freeman 2010). It has been estimated that a single mature rodent astrocyte can encompass between 20,000-80,000 μm^3 of domain space, wrap many neuronal somatas, associate with 300-600 neuronal dendrites, and make contacts with more than 100,000 single synapses (Freeman, 2010). These findings are underscored by the fact that a single mature human astrocyte holds 30 times the volume as a rodent, making contact with over 2,000,000 individual synapses (Freeman, 2010; Oberheim et al., 2006). During the first post-natal week of development, immature astrocytic cellular processes begin to sprout and processes actively elongate (Freeman, 2010). The local immature astrocytes also tend to have overlapping processes. By 2 post-natal weeks, these overlapping processes are "pruned" and develop more distinct borders (Freeman, 2010). At around 3-4 post-natal weeks these processes significantly increase in the degree of branching, with more distal processes becoming thinner and spongiform, and even finer processes densely infiltrating the brain (Freeman, 2010). The spatial domains also become even more resolved, with very little overlap between adjacent astrocytes. It is around this time that astrocytes are considered to have a "mature" morphology. Despite the complexity and large amount of coverage provided by a single astrocyte, little is known about the signaling pathways controlling the morphological maturation process that occurs during the transition of an immature to mature astrocyte (Freeman, 2010).

It has only recently been discovered that astrocytes express MeCP2 (Ballas, Lioy, Grunseich, & Mandel, 2009; Maezawa, Swanberg, Harvey, LaSalle, & Jin, 2009). Initial studies utilizing primary cultures of astrocytes and neurons demonstrated that *MeCP2*-deficient astrocytes are not capable of supporting normal neuronal cell growth and

morphology (Ballas et al., 2009; Lioy et al., 2011). Wildtype (WT) neurons cultured with *MeCP2*-deficient astrocytes displayed reduced spine number and stunted dendrites (Ballas et al., 2009; Maezawa et al., 2009). Inducible knock out of MeCP2 specifically from astrocytes recapitulates several phenotypes observed in global *MeCP2*-deficient mice, including abnormal breathing patterns, reduced body size and hind-limb clasping (Lioy et al., 2011). Post-natal re-expression of MeCP2 in astrocytes ameliorates breathing abnormalities, restores neuronal soma size and dendritic complexity, restores body weight, improves life span, and ameliorates anxiety-like behaviors in *MeCP2*-deficient mice (Lioy et al., 2011). These studies suggest astrocytes play a significant role in the pathogenesis of Rett syndrome. Surprisingly, the mechanism by which astrocytes contribute to RTT has received little attention, however; a recent study has implicated astrocyte morphology in mouse model of RTT. In this study the authors utilized an inducible post-natal knock down of MeCP2 to examine the effects of MeCP2 loss at two different stages: late juvenile stage and adult stage. Interestingly they report that MeCP2 loss at the two time points results in equal symptoms. Their studies found that post-natal loss of MeCP2 in late juvenile or adult healthy male mice resulted in brain shrinkage, increased neuronal cell density, retraction of dendritic arbors, decreased dendritic spine density, and most importantly for our studies, decreased astrocyte processes complexity (Nguyen et al., 2012). To investigate astrocyte complexity they used a modified Golgi technique, specifically the Golgi-Cox method, followed by Sholl analysis. Loss of MeCP2 resulted in a decrease in astrocyte complexity, decreased number of nodes, and decreased mean length of astrocyte processes in the CA1 region of the hippocampus. It is worth noting in these studies that MeCP2 was ablated from animals at six weeks of age

and images were acquired at 24 weeks of age. This late developmental ablation of MeCP2 may not fully reflect the human condition in which the mutation is present throughout all phases of development or other animal models of RTT that utilize global knockout of gene expression. Regardless, these studies suggest that MeCP2 expression is required for astrocytes to maintain normal morphology.

HYPOTHESIS

In this study we test the central hypothesis that MeCP2 deficiency in the brain prevents astrocytes from attaining proper, mature morphological complexity and/or decreased cell numbers in the RTT brain. The consequences of which would alter brain development and contribute to overall decreased brain volume observed in humans with RTT and animal models of the disease.

METHODS

Animals: All experimental protocols were performed in accordance with the NIH guidelines and were carried out with the approval of the Animal Care and Use Committee of the University of Alabama at Birmingham (Animal Permit Number: 09409). Experimental animals were littermates bred in our animal facility by crosses of $Mecp2^{ZFN/+}$ females (SD- $Mecp2^{tm1sage}$) to wildtype (WT) S100β eGFP (enhanced green fluorescent protein) males obtained from the National Bioresource Project Rat (Japan) [Itakura, E., Odaira, K., Yokoyama, K., Osuna, M., Hara, T. and Inoue, K. (2007] For the purpose of this study the rats have astrocytes that express eGFP (Nwaobi et al., 2014). All rats were genotyped for MeCP2 deletion by PCR using DNA obtained from tail snips and Clontech's Terra PCR Direct Genotyping kit. Primers used were the following: forward 5- GCAGCATCAGAAGGTGTTCA-3 and reverse 5-GACCTCAATGCTGACGGTTT-3. Expected bands were as follows: WT = 345bp and $Mecp2^{ZFN/y}$ =247bp. Muller glia of the retina express S100β, thus these animals were identified by eGFP fluorescence under black light, negating the need for genotyping. All animals were housed under standard 12-hour-light-dark cycles.

The Rett rat model

While mice have been the preferred species for Rett syndrome studies in the past, the development in the ability to manipulate the rat genotype has presented several advantages and opportunities with using rats for the study of the disorder. The large size of the rats in comparison to mice allow for better identification of early disease development and expression. In later stages electrophysiological studies, direct drug

delivery, and surgery are applied more easily because of the anatomical size. The size difference also allows consideration of the importance of structure size in age dependent and region specific studies related to the central nervous system (Patterson, Hawkins et al. 2016).

The more complex cognitive and social behavioral structure of rats is also an advantage for use in Rett syndrome studies, due to the importance of cognitive impairment and time points with the syndrome (Panksepp 1981, Thor and Holloway 1984, Pellis and McKenna 1995, Pellis and Pellis 1997, Pellis and Pellis 1998, Urcelay and Miller 2010, Battaglia, Borensztajn et al. 2012). As a result of the advantages, Sage laboratories generated the rat model by modeling its motor and behavior to that of existing mouse and human Rett syndrome patients. Using zinc-finger technology a 71 base pair deletion was generated in the fourth exon of the Mecp2. These male knockout rats express no functional Mecp2 protein, while female heterozygous animals express approximately 50% of their wildtype female littermates (Patterson, Hawkins et al. 2016). Throughout the remainder of this text we will refer to phenotypes in male knockout rats, as they were the models used in this study.

During the course of post-natal development, wet brain weights revealed that MeCP2 rat brains, like that of humans and murine models of the disease, weigh significantly less than wildtype animals by post-natal date 14 (PND 14). MeCP2 rats began to show symptoms in their early developmental stages; in comparison to their littermates, they displayed lethargic behavior with abnormal fur appearance. By post-natal date 55, approximately one half of the males had died (Patterson, Hawkins et al. 2016).

A phenotype comparison between the male rat model of RTT and mouse models of the disease demonstrate many similarities, however, in many instances the rats displayed symptoms at earlier time points than those reported for mice, which is more reflective of human RTT. Primary phenotypes, other than reduced brain weight included reduced motor coordination by post-natal day (PND) 21-28+ and presentation of a tremor occurred by PND 21. Hypoactivity, abnormal gait and breathing abnormalities were also observed at PND 21-28+ (Patterson, Hawkins et al. 2016). This data indicates that the rat is a valid model to study this disease, and because of its larger size may represent a superior model.

Tissue collection and sectioning: All animals were harvested at post-natal day 30 ± 2 days (a time point in which the animals were considered symptomatic) by transcardial perfusion with 4% PFA. After perfusion brains were allowed to soak in 4% PFA for at least 24 hours before being switched to a 30% sucrose (in PBS) solution. Brains were allowed to sink in sucrose for 48 hours prior to being frozen in OCT for cyrosectioning. To hasten the freezing process the cyromolds were placed in a 100% ethanol-dry ice slurry. 50 μm sagittal sections were cut at -15°c, then free floated in PBS.

Golgi Staining: To preferentially stain glia cells over neurons, tissue was incubated in the modified Golgi-cox solution for 48 hours at 37°C as previously described in (Ranjan 2012, Rutledge 1969). The Golgi- cox solution was made as previously described (Rutledge 1969) composing of 40 parts distilled water, 20 parts 5% potassium dichromate, 16 parts 5% potassium chromate, and 20 parts 5% mercuric chloride. This solution was made fresh for each use. The perfused brains were allowed to soak in this solution for 48 hours at 37°C in the dark. Following incubation the brains were rinsed

with PBS to remove any excess Golgi-cox solution before being placed in 30% sucrose in PBS for 48 hours at 4°C before being cyrosectioned. As described above the tissue was cyrosectioned in 50μm sagittal sections and free-floated in PBS. The Golgi-impregnated tissue was then dehydrated and cleared before being mounted on slides. The dehydration protocol was strictly adhered to as described by Ranjan (Ranjan 2012). Sections were dehydrated in 50% ethanol for 5 minutes then transferred to a 3:1 ammonia to distilled water solution for 10 minutes. Followed by two 5 minute rinses with distilled water and treatment with 5% sodium thiosulfate for 10 minutes in the dark. The sections were rinsed in distilled water twice for 2 minutes, then dehydrated twice in 70%, 80%, 95%, and 100% ethanol for 5-10 minutes each. Lastly the tissue was cleared in toluene twice for 15 minutes then mounted on slides with distrene plasticizer xylene (DPX) mounting solution (Ranjan 2012).

Immunohistochemistry: Slices were incubated in blocking buffer (10% goat serum, 0.3% Triton-X-100 in PBS) for 1 hour at room temperature, followed by incubation in primary antibodies [overnight at 4° C rabbit anti Glial Fibrillary Acidic Protein (GFAP) (Dako Z0334, 1:500) and mouse anti Neuronal Nuclei (NeuN) (Millipore MAB377, 1:500)]. The slices were then washed in diluted blocking buffer (1:3 dilution) for 3 x 15 minutes and incubated in secondary antibodies (Alexa Flour 1:500) for 1 hour at room temperature. Slices were then washed again with diluted blocking buffer 4 x 5 minutes and the cell nuclei stain DAPI (1:10,000 in PBS) was added for 5 minutes followed by a 5 minute wash in PBS. Slices were then mounted on charged slides using Sigma Flouromont (F4680 Sigma)

Microscopy: Immuno labeled fixed slices were imaged on a Nikon A1R confocal. High resolution images were taken with a 60x oil immersion lens. Images were taken with four lasers: 405nm, 488nm, 561nm, and 647nm using the Nis Elements 4.50 Imaging Software. The same volume was acquired for all slices using the same step size of 0.45 μm for a total of 40 μm. Analysis was performed on compressed images.

Bright field images were taken using a Zeiss Axio Examiner D1 microscope with a 10x air lens to visualize the Golgi impregnated cells. AxioVision 4.8.2.0 software was used to acquire images.

Data Analysis: GraphPad Prism (v. 5.02) software was used to graph and analyze results. Two-way ANOVA, followed by a Bonferroni posttest, was used to determine significance with *a priori* alpha value of 0.05. For data sets with only two parameters tested, an unpaired t-test was used $p < 0.05$ was used as the cut off for significance.

Processing of bright field images prior to Sholl analysis was done as follows. The contrast of the images was optimized before being converted to binary images via ImageJ (Process > Binary > Make Binary). Images were further processed to ensure that the image used for Sholl analysis was composed of one individual cell. When additional cells were too close to crop out, they were drawn over with the ImageJ paintbrush feature. Astrocytes were identified by their morphology as previously described (Nguyen, Du et al. 2012). In the case that parts of the astrocyte were lost in the binary processing, the deleted branches were drawn in to the furthest remaining portion. Branches were never completed past the furthest remaining portion. This was done to ensure no results were exaggerated. We believe this in turn caused the astrocytes to appear smaller and potentially less complex, but for the integrity of the results this was a reasonable trade-off

(Kutzing, Langhammer et al. 2010). Following the image processing mentioned above, Sholl analysis on each individual cell from both genotypes was performed using the Image J Sholl plug in. The Sholl analysis plugin is a free plugin made publically available by the NIH and ImageJ imaging software. This plugin was first used by Ferreira et al. in 2010 (Ferreira, Iacono et al. 2010). This software generates a series of concentric circles around a predefined starting location and counts the number of intersections on each of the rings. The software output consists of multiple quantifiable parameters related to cell complexity including: ending radius, total intersections, median intersections, enclosing radius and regression coefficient, to name a few. Below we have cartooned each of these parameters for demonstration (Figure 1). The blue points seen in Figure 1 represent the primary branch points. The orange points represent intersections of the image of interest and the concentric rings, number of intersections vs. distance from the soma and total number of intersections are determined from these points. Finally, the yellow line in Figure 1 represents the maximum length of a process that extends from the cell soma that was used to quantify the average maximum length analysis.

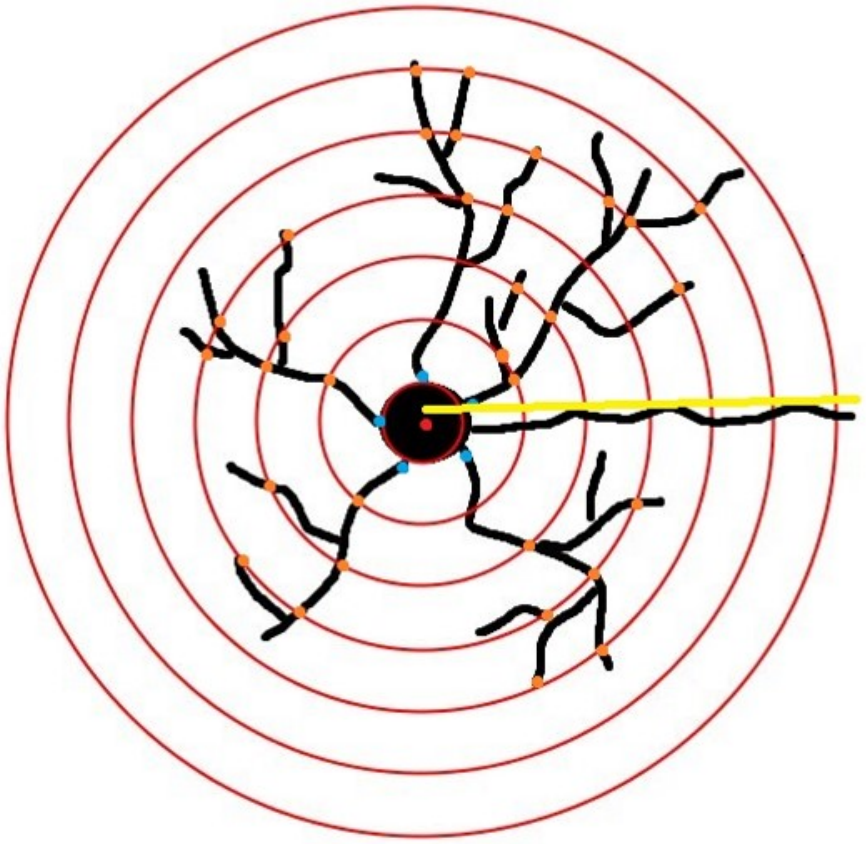

Figure 1. Cartooned example of an ideal single cell demonstrates the parameters analyzed using Sholl analysis. This image was free drawn in Photoshop and the ImageJ plugin. Concentric circles was used to overlay the circles on top of the image. The blue dots represent primary branches while the orange dots represent other intersections. The yellow line represents the maximum length of a process from the soma.

RESULTS

Hippocampal Astrocyte Complexity in a Rodent Rett Syndrome Model

In order to begin addressing the hypothesis that astrocytes exhibit altered morphological complexity, Sholl analysis was performed on Golgi labeled astrocytes from the CA1-CA2 regions of the hippocampus. To determine if loss of function of MeCP2 protein from embryonic development, as would occur in the human disease, results in similar astrocyte deficits as previously reported in late juvenile knockdown models. CA1-CA2 hippocampal astrocyte morphology was examined in symptomatic (P28-P30) RTT rats. Representative bright field images of Golgi impregnated hippocampal CA1-CA2 astrocytes from wildtype and MeCP2 KO rats are shown (Figure 2). Their representative processed images were generated for the purpose of automated Sholl analysis are also shown in Figure 2 underneath their respective bright field images.

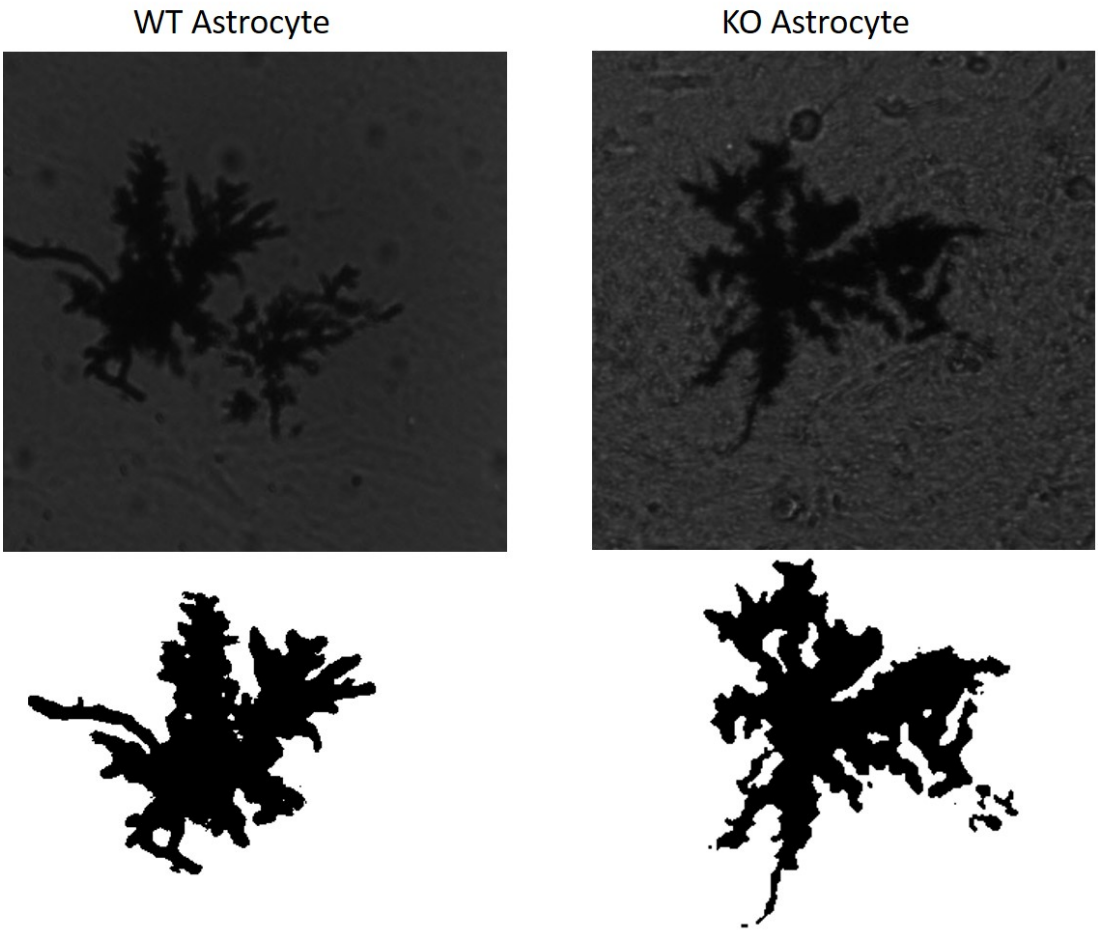

Figure 2. Representative 10x images of hippocampal Golgi-labeled astrocytes. The upper two images are the images obtained from the bright field microscopy, while the bottom two images are the same cells post-processing for automated Sholl analysis.

Mean data obtained from genotype blinded analysis revealed there was no statistical difference in the number of intersections per distance from the soma between wildtype and MeCP2 knockout rat littermates' astrocytes at any distance from the center of the soma. Analyzed data obtained from Sholl analysis (Figure 3) showing the number of intersections per distance from the soma reveals no difference between wildtype and knockout animals at any distance from the center of the soma. A two way paired ANOVA was done followed by a Bonferroni post–hoc test. n = 20 for wildtype animals and n = 25 for knockout animals, each group coming from 3 animals.

Additionally hippocampal astrocyte average maximum length, average primary branches, and total intersections were examined (Figure 4). An unpaired t-test revealed no detectable differences in any of these parameters. The average maximum length for wildtype astrocytes was 106.5 μm ± 7.832 while the average maximum length for MeCP2 knockouts rats was 103.9 μm ± 7.301. The average number of primary branches for wildtype and Mecp2 knockout astrocytes were 4.150 ± 0.1957 and 4.360 ± 0.2301 respectively. Lastly the total number of intersections for wildtype and MeCP2 knockout astrocytes were 90.79 ± 7.552 and 86.76 ±7.898 respectively. This data indicates that there was no statistical difference in astrocyte complexity between wildtype and RTT CA1-CA2 hippocampal astrocytes.

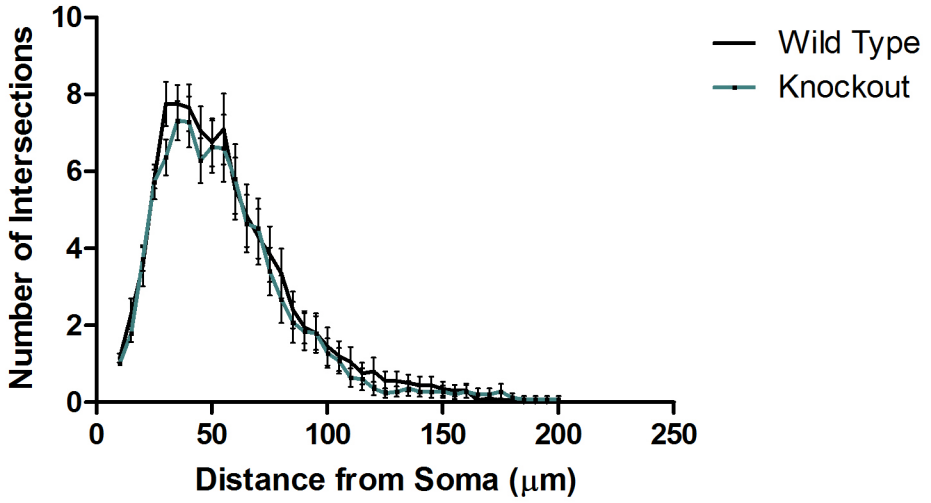

Figure 3. Astrocyte complexity at defined distances from the cell soma are not different between wildtype and symptomatic MeCP2 knockout astrocytes in the CA1-CA2 hippocampal region. A two way paired ANOVA followed by a Bonferroni posttest showed no statistical differences in the number of intersections vs. distance from the soma between wildtype and MeCP2 knockout rat hippocampal astrocytes from the CA1-CA2 region. A total of n = 20 wildtype and n = 25 Mecp2 knockout astrocytes (3 animals per genotype) were examined.

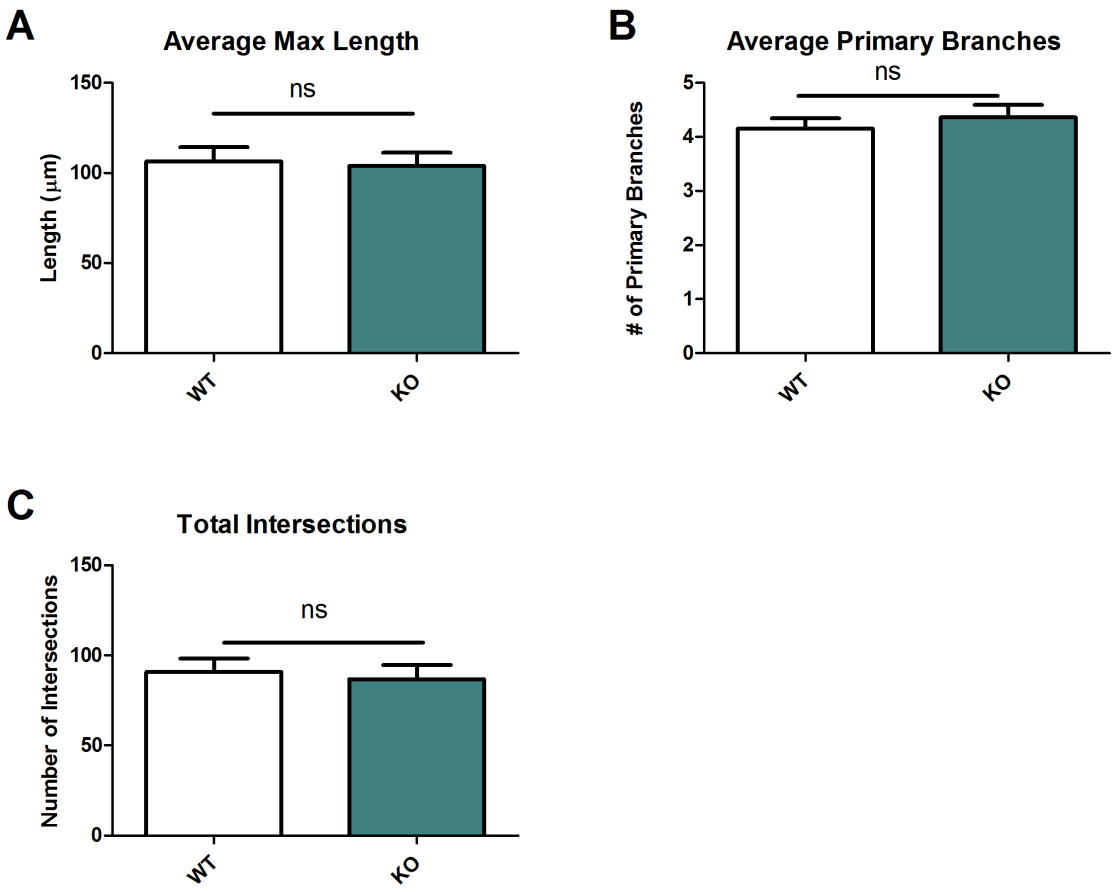

Figure 4. Astrocyte complexity is not different between wildtype and MeCP2 symptomatic astrocytes in the CA1-CA2 hippocampal region. (A) There was no difference between the average max length of wildtype and knockout astrocytes. (B) There was also no difference between the number of primary branches of wildtype and knockout astrocytes. (C) Lastly there was no difference in total number of intersections between wildtype and knockout hippocampal astrocytes A total of n = 20 wildtype and n = 25 Mecp2 knockout astrocytes (3 animals per genotype) were examined.

Astrocyte Cell Numbers in RTT Hippocampus and Cortex

Previous studies have reported various abnormalities involving the RTT brain, with an emphasis on neuronal populations. To date however there are no published works examining astrocyte number and density. Next astrocyte cell numbers in CA2-CA1 of the hippocampus were evaluated, the molecular layer of the hippocampus, and the upper cortical layers (Layer II/III of the motor cortex). The selection of the motor cortex was based on the observation of the complexity and motor-sensory integration, which show deficits in RTT (NK Casanova et al 1991). Human MRI studies indicate abnormalities in the cortex (NK Casanova 1991, Gotoh, Naidu). Furthermore, in murine models of the disease, cortical layer II/III pyramidal neurons display significantly less complex dendritic arbors when compared to WT littermates.

Cell counts in layer II/III of the motor cortex were performed and CA1-CA2 region of the hippocampus. Representative images from the hippocampus for wildtype and MeCP2 knockout animals are shown below (Figure 5). The images show the nuclei stain DAPI in blue, S100-β eGFP in green, GFAP in red, and NeuN in white. Six images were taken from each region of interest per genotype from three different animals. The number of DAPI positive cells were determined, eGFP and GFAP positive cells, and NeuN positive cells. While both S100-β and GFAP are present in some other cell populations, the presence of both were utilized to conclusively determine astrocyte counts. These mean counts obtained from each of these images are shown in Figure 6. No difference in the total number of DAPI positive cells per 100 μm^3, the total astrocyte

number per 100 μm^3, total neuron number per 100 μm^3, astrocyte to total cell ratio, or astrocyte to neuron ratio were observed between wildtype and symptomatic MeCP2 knockout littermates, in the hippocampal CA1-CA2 region. The mean DAPI positive cell was not different between wildtype and MeCP2 knockouts (63.675 ± 6.879 and 65.245 ± 7.012 respectively) (Figure 6A). The mean astrocyte numbers per 100 μm^3 for wildtype and knockouts were 35.48 ± 3.827 and 30.93 ± 2.404 respectively, with a *p* value of 0.0512 (Figure 6B). The mean neuron numbers per 100μm^3 were 3.402 ± 0.5611 for the wildtype animals and 4.754 ± 0.4853 for the knockout animals (Figure 6C). The mean astrocyte to total cell ratio was 0.5537 ± 0.05310 and 0.4849 ± 0.03011 respectively, which was not significantly different (Figure 6D). The mean astrocyte to neuron ratio in the hippocampus was 12.11 ± 2.447 and 6.638 ± 0.3516 respectively ($p = 0.0512$) (Figure 6E). The data indicates that while independently none of these values were significantly different, there is a trend towards a decrease in total astrocyte per 100 um^3, astrocyte normalized total cells, and astrocytes normalized to neurons. All groups were analyzed with a non-paired student's t-test.

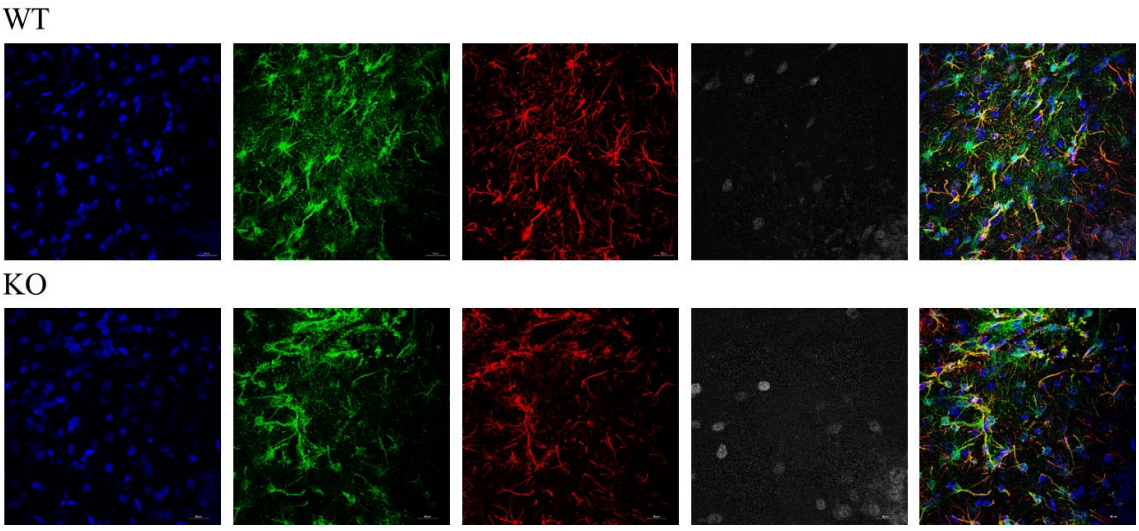

Figure 5. Representative wildtype and MeCP2 knockout images from CA1–CA2 hippocampus regions. The upper row of images shows a series of representative wildtype images. In blue is a nuclear DAPI stain. In green is eGFP –S100β. In red is a GFAP staining. In white is a NeuN staining. The last image is merge of all four channels. The lower row of images shows a series of representative knockout images.

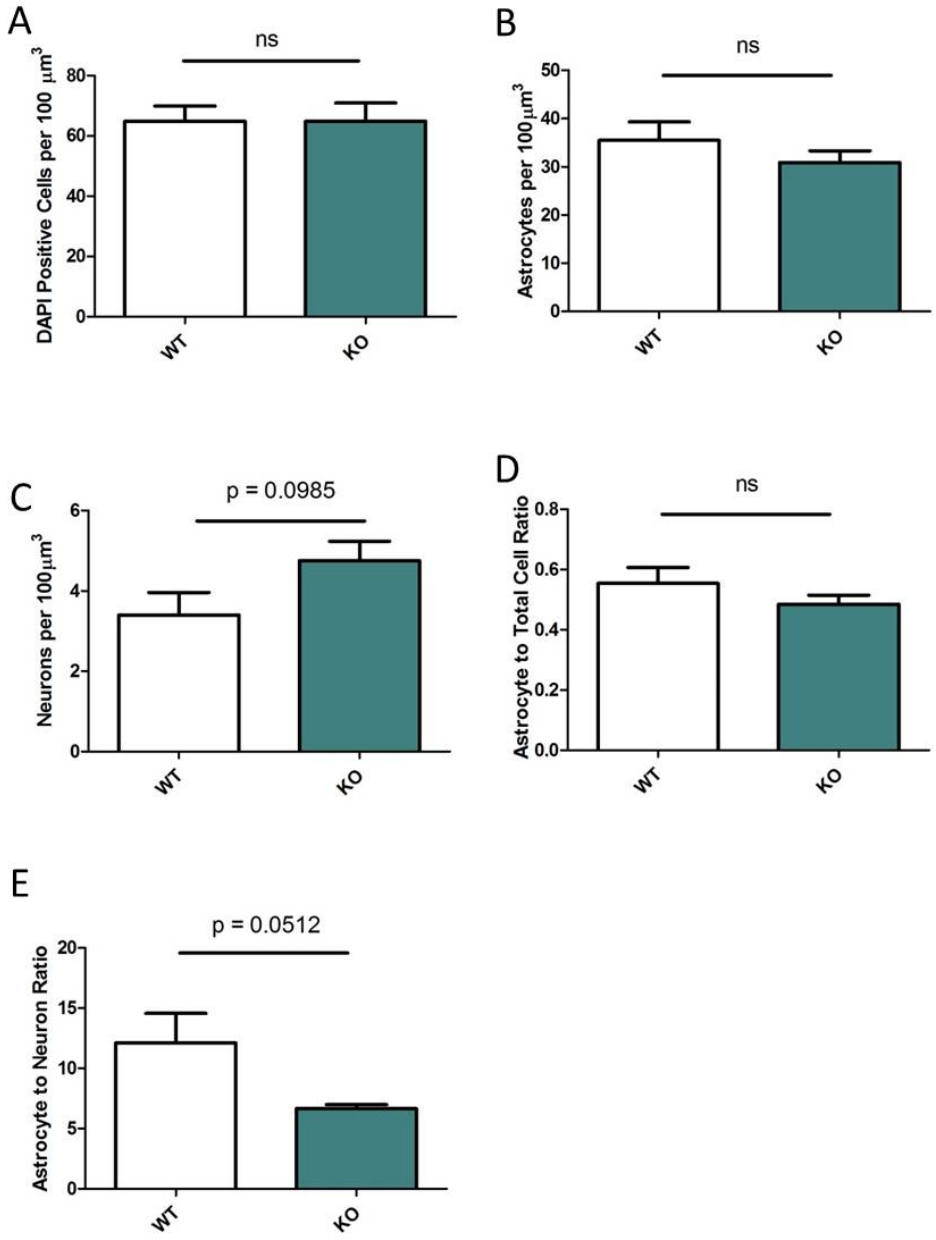

Figure 6. Hippocampus cell counts. (A) Analysis showed no significant difference in the number of total number of DAPI positive cells per 100 μm^3 in the hippocampus. (B) The difference in number of astrocytes per 100 μm^3 was not significant. (C) The number of neurons per 100 μm^3 trended towards an increase with a p value of 0.0985. (D) The astrocyte to total cell ratio was not different. (E) The astrocyte to neuron ratio while not significantly decreased had a p value of 0.0512. n = 6 from 3 animals per genotype. $p < 0.05$

The astrocyte population of layer II/III of the motor cortex was also assessed. Representative images of layer II/III of the motor cortex for both wildtype and knockout animals can be seen below in Figure 7.

As previously done in the Hippocampus, the same analysis was done in the motor cortex. The total number of DAPI positive cells per 100 $100\mu m^3$ was not different between wildtype and RTT animals (98.768 ± 9.543 and 85.267 ± 8.124 respectively) (Figure 8A). The total number of astrocytes per $100\mu m^3$ in wildtype and knockout animals with means of 9.754 ± 1.444 and 15.41 ± 2.690 respectively, were not significantly different, although there was a trend towards an increase in astrocyte number in the motor cortex with a *p* value of 0.0938 (Figure 8B). There was no difference detected between the total number of neuron per $100\mu m^3$ between the wildtype animals with a mean of 65.30 ± 4.514 and RTT animals with a mean of 64.77 ± 4.354 (Figure 8C). There was a significant difference between the astrocyte to total cell ratio in the motor cortex of wildtype and RTT animals with mean ratios of 0.09899 ± 0.008666 and 0.1509 ± 0.02078 respectively with a *p* value of 0.0437 (Figure 8D). There was no significant difference between wildtype and RTT astrocyte to neuron cell ratios in the motor cortex with mean ratios of 0.1471 ± 0.01945 and 0.2381 ± 0.03924 respectively (Figure 8E). However, there was a trend towards a rise in astrocyte to neuron ratio in the motor cortex in knockout animals with a p value of 0.0669.

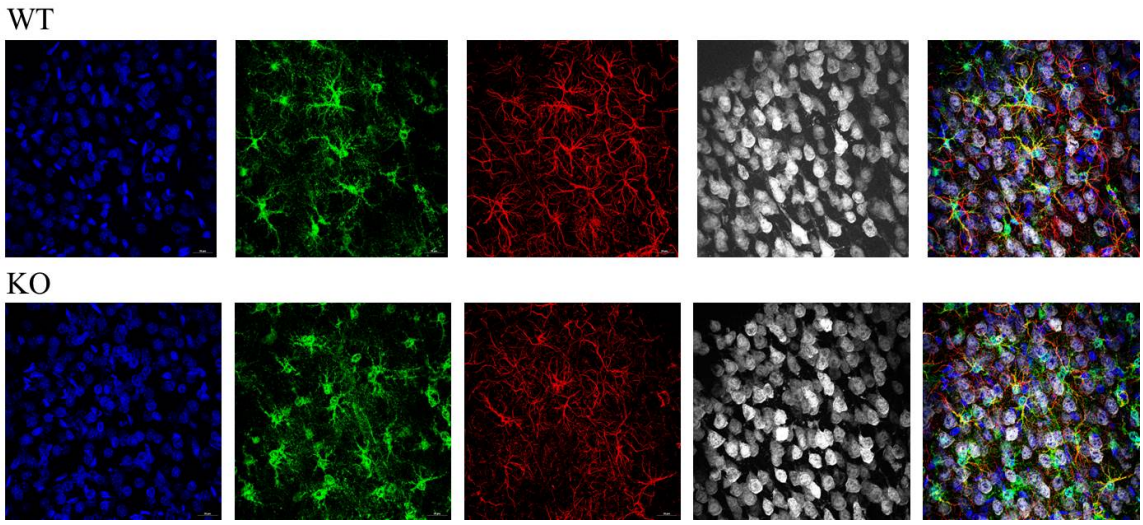

Figure 7. Representative wildtype and MeCP2 knockout images from the motor cortex. The upper row of images shows a series of representative wildtype images. In blue is a nuclear DAPI stain. In green is eGFP –S100β. In red is a GFAP staining. In white is a NueN staining. The last image is merge of all four channels. The lower row of images shows a series of representative knockout images.

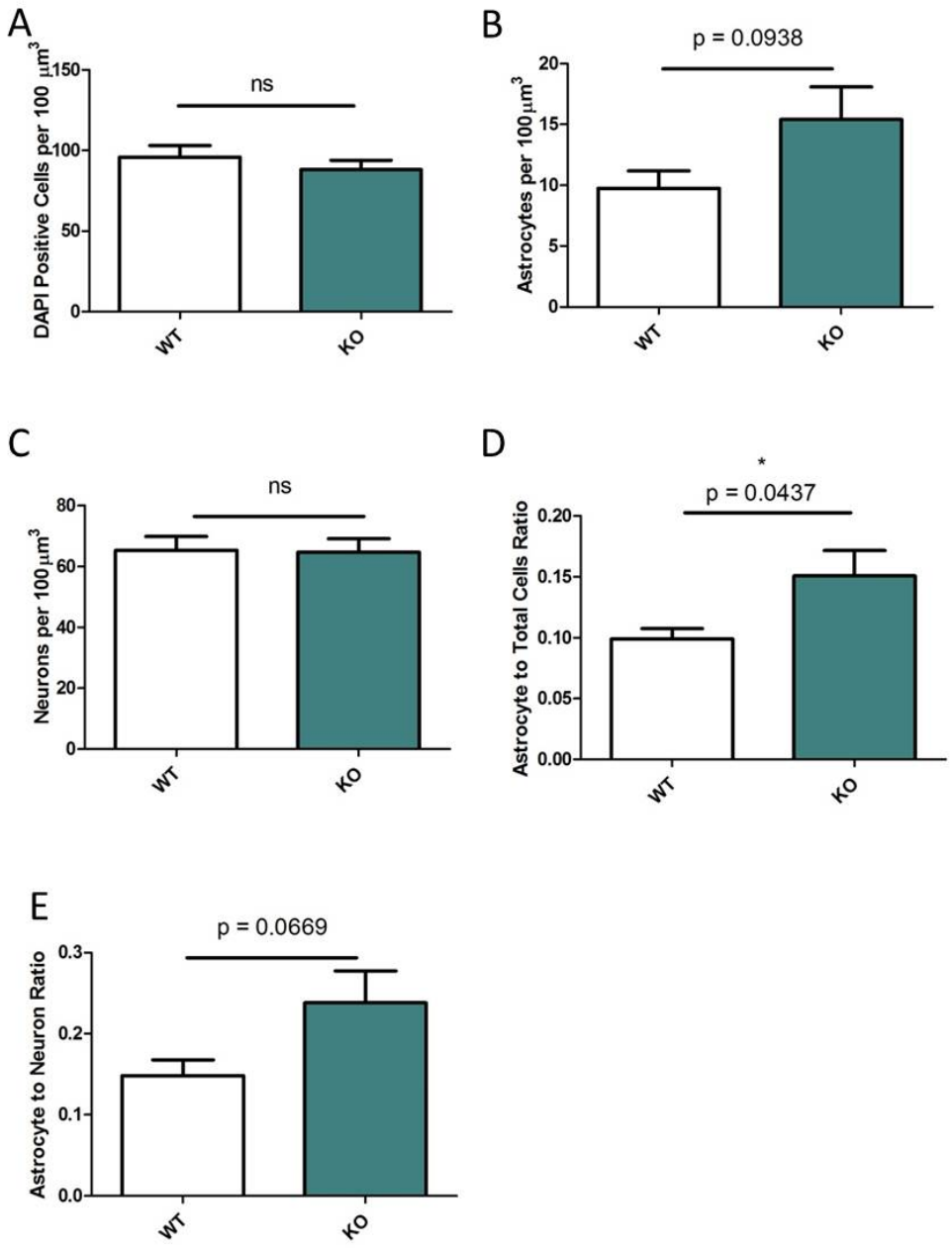

Figure 8. Motor cortex cell counts. (A) Analysis showed no significant difference in the total number of DAPI positive cells per 100 μm^3 in the hippocampus. (B) The difference in number of astrocytes per 100 μm^3 was not significant, but was trending towards an increase. (C) The number of neurons per 100 μm^3 was not different. (D) The astrocyte to total cell ratio was increased. (E) The astrocyte to neuron ratio while not significantly decreased had a p value of 0.0669. n = 6 from 3 animals per genotype. $p < 0.05$

DISCUSSION

The current study was the first study to address astrocyte cell complexity and astrocyte cell numbers in a rodent model of the neurodevelopmental disorder Rett syndrome. Blinded Sholl analysis of CA1-CA2 hippocampal astrocytes indicates no difference in average maximum length, the number of primary branches, or the total number of intersections between wildtype and MeCP2 knockout astrocytes. Furthermore, there was no difference in number of intersections at any distance from the soma when comparing wildtype and MeCP2 knockout astrocytes. This data indicates that in CA1-CA2 of the hippocampus, there is no difference in astrocyte complexity between wild type and symptomatic MeCP2 KO rat littermates. In contrast we observed a trend toward reduced total astrocytes, astrocyte to total cell ratio, and astrocyte to neuron cell ratio in the CA1-CA2 region of the hippocampus. While in the motor cortex the opposite was observed, with a trend of increased total number of astrocytes and astrocyte to neuron cell ratio observed. The number of astrocytes to total cell ratio was significantly increased in motor cortex. Together this data indicates that differences in astrocyte cell numbers, rather than morphological complexity, may contribute to astrocyte-associated dysfunction in Rett syndrome. Although not assessed in this study differences in gene expression and protein expression have been reported in murine models of the disease (Alvarez. 2007). Further study is warranted to determine if changes in astrocyte cell number contribute to observed changes in gene and protein expression.

Caveats to Determining Morphological Complexity of Astrocytes in Rett Syndrome

The 'shadow' effect

Astrocyte morphology is extraordinarily complex, as detailed in the introduction. Traditional intermediate process labeling demonstrates long filamentous processes, however, recent data has indicated that astrocytes have a more "bushy" like appearance (Bushong, Martone et al. 2004). Bright field images of Golgi labeled cells revealed a shadow effect, making branch points difficult to discern (Figure 2). To combat this issue we attempted to take advantage of reflective properties of metals used in the Golgi impregnation, and perform reflective confocal microscopy. Astrocyte images acquired using this method proved to be as 'bushy' (not shown) and this method was abandoned due to the increased time requirements for image acquisition. We do believe the shadow effect led to an underestimation of overall astrocyte complexity. However, even at the most extreme distances from the cell soma, where the shadowing effect was minimized due to fewer numbers of processes, no differences in intersections or overall maximum length of processes was observed. These findings make it unlikely that the shadow effect masked real differences in complexity between the two genotypes.

Taken at face value, our data indicates that changes in morphological complexity of astrocytes in the hippocampus in symptomatic MeCP2 rats do not account for alterations in hippocampal function. This data is in contrast to those published in a murine model, where MeCP2 was ablated in late juvenile animals (Nguyen, Du et al. 2012). These discrepancies may relate to the timing to the deficiency in MeCP2 protein function. It is possible that MeCP2 is not required for astrocytes to attain a mature morphology, but rather is required for long-term maintenance of their morphology. An

alternative explanation may be that the animals in our study were collected relatively early in the disease progression at post-natal day 30. The mice, which showed changes in astrocyte morphology, were collected at 24 weeks. In comparison our rats have reached a 50% mortality by 6 weeks (Patterson et al. 2016). Finally, the differences in species between the two studies may account for the differences observed.

Complexity of astrocytes in the superficial cortical layers

We initially planned to perform Sholl analysis in both the motor cortex and CA1-CA2 region of the hippocampus upon impregnation with Golgi solution. However, increased labeling density was observed in the motor cortex, making it impossible to separate one astrocyte from the other. It is unclear why cells in this region labeled at a higher frequency than hippocampal astrocytes. This may be related to being situated closer in proximity to the pial surface of the brain, allowing greater access to impregnation solution. Future experiments aimed at labeling cells in this region may require reduced time in the Golgi impregnation solution. An alternative strategy would utilize individually dye-filling astrocytes in the desired region.

Analysis of area and perimeter of hippocampal astrocytes

In an attempt to address the issue of the "shadow" effect seen in the golgi impregnated astrocytes we did some further analysis of the individual astrocytes. As an alternative method of assessing astrocyte complexity while not being affected with the lack of clarity we assessed the area and perimeter of the astrocytes. When assessed we found no difference in the area or perimeter between wildtype and knockout (Figure 9.). The wildtype astrocytes have an average area of 6448 $\mu m^2 \pm 553.2$ compared to the 6567

μm^2 ± 723.2 for the MeCP2 knockout astrocytes. The perimeter for the wildtype astrocytes were 1069 μm ± 88.42 compared to 1016 μm ± 80.25 for the Mecp2 knockout astrocytes. This data in conjunction with the Sholl analysis data we are pretty confident there is no difference in astrocyte complexity in wildtype and Mecp2 deficient animals.

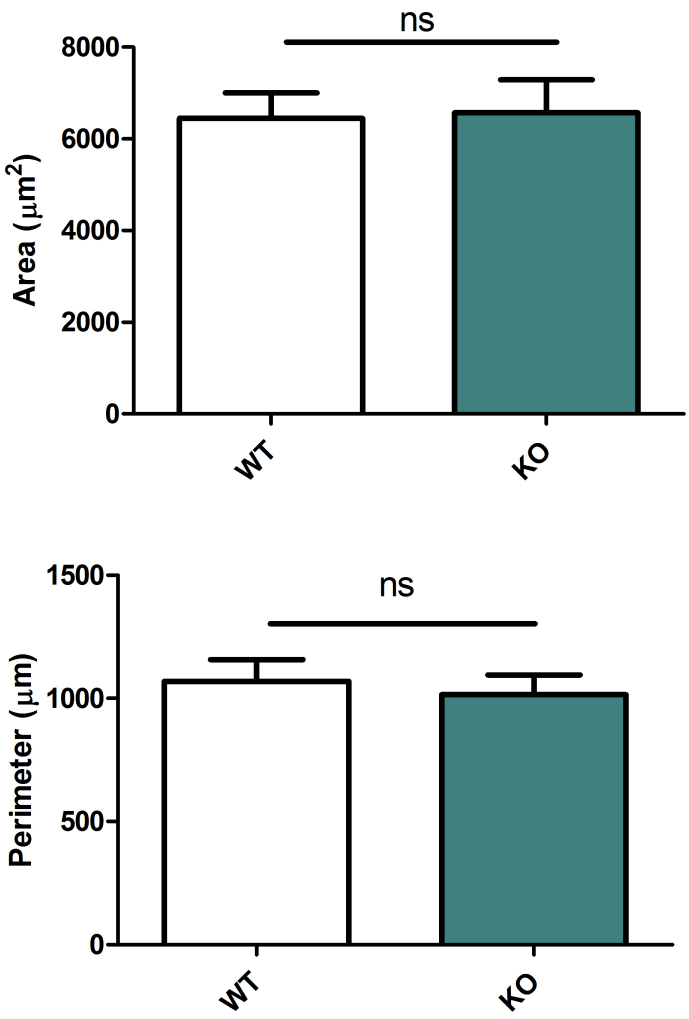

Figure 9 Astrocyte area and perimeter are not different in MeCP2 deficient astrocytes. There was no difference in area between wildtype and knockout astrocyte (top panel). There was also no difference in perimeter between wildtype and knockout astrocytes (bottom panel). A total of n = 20 wildtype and n = 25 Mep2 knockout astrocytes (3 animals per genotype) were examined.

Quantifying Astrocyte Cell Number in the Hippocampus and Motor Cortex

To date no study has examined astrocyte cell numbers in any brain region in any of the available models of RTT or human RTT patients. However, increased neuronal cell densities were observed in cortex and hippocampus in MeCP2 deficient mice (Nguywen et al. 2012, Kishi & Macklis, 2004). Given that thinning of both tissues in MeCP2 mice has been reported, it is conceivable that increased neuronal density occurs at the expense of fewer astrocytes. Indeed this may be the case in the hippocampus where all parameters measured regarding astrocyte cell numbers converged towards statistical significance. Interestingly the complete opposite trend was observed in the cortex. Further studies in additional animals are needed to determine if these trends represent real changes in astrocyte numbers between wildtype and early symptomatic Mecp2 deficient rats, as this would have important ramifications on gene expression profiling and subsequent protein expression studies between these two brain regions in RTT. Further, these differences may contribute to differences in excitability in the two regions.

Future Studies

While not complete, these studies are novel and lay the groundwork for future work aimed at examining astrocyte cell numbers and complexity in animal models of Rett syndrome. As mentioned in the previous section we think it is important to perform additional studies examining astrocyte cell numbers between wildtype and Mecp2 KO rats given the trends we observed. Future studies should be extended to examine animals later in the course of their disease, as well as incorporate female animals into our studies. Female heterozygous animals represent the more clinically appropriate model of RTT.

However, the majority of basic research has focused on male hemizygous animals. This is largely due to the consistent onset of early disease symptoms and rapid disease progression in male knock out animals that express no functional MeCP2 (Schaevitz, Gomez et al. 2013). In contrast female heterozygous animals display a much later onset of symptoms (4-6 months rather than 4-6 weeks). Additionally, as mentioned in the introduction, the *MeCP2* gene is located on the X chromosome and subject to X chromosome inactivation. This leads to a mosaic pattern of MeCP2 expression and introduces variability in symptom onset and disease progression in females that adds additional complexity when using this model. It must be noted that even female RTT animals do not represent an ideal model, as they do not develop symptoms until well into adulthood (4-6 months) which, fails to model the neurodevelopmental aspect of RTT. Regardless, reduced brain weights are observed in human RTT female patients and female models of the disease (Bauman, Kemper et al. 1995, Jentarra, Olfers et al. 2010) including the RTT rat model (Patterson, Hawkins et al. 2016). It is possible that in the male rodent model of the disease, they reach the terminal stage of the disease so quickly that astrocyte morphology does not have the 'time' to change. In contrast female heterozygous RTT animals (and human patients) have a relatively normal lifespan. This protracted disease progression may allow for exaggerated changes in astrocyte cell numbers and morphology not observed in early juvenile male rats.

Finally, we believe that to accurately address changes in astrocyte morphology, a dye filling technique should be utilized. This technique would allow for proper confocal microscopy, which would negate the shadowing effect as well as letting us visualize a

complete astrocyte with no under representation. This would also make it possible to do 3D volume analysis, which would be an excellent marker for astrocyte complexity.

We believe this body of work is useful at directing future studies, leading to a better approach for addressing astrocyte morphology and cell numbers in RTT. We think this study brings light to the need for additional techniques to analyze astrocyte morphology and complexity.

Reference List

Alvarez-Saavedra, M., Saez, M. A., Kang, D., Zoghbi, H. Y., & Young, J. I. (2007). Cell-specific expression of wild-type MeCP2 in mouse models of Rett syndrome yields insight about pathogenesis. Hum.Mol.Genet., 16, 2315-2325.

Amir, R. E., Van den Veyver, I. B., Wan, M., Tran, C. Q., Francke, U., & Zoghbi, H. Y. (1999). Rett syndrome is caused by mutations in X-linked MECP2, encoding methyl-CpG-binding protein 2. *Nat Genet, 23,* 185-188.

Armstrong, D., Dunn, J. K., Antalffy, B., & Trivedi, R. (1995). Selective dendritic alterations in the cortex of Rett syndrome. *J.Neuropathol.Exp.Neurol., 54,* 195-201.

Armstrong, D. D., K. Dunn and B. Antalffy (1998). "Decreased dendritic branching in frontal, motor and limbic cortex in Rett syndrome compared with trisomy 21." J Neuropathol Exp Neurol 57(11): 1013-1017.

Armstrong, D. D. (2005). Neuropathology of Rett syndrome. *J.Child Neurol., 20,* 747-753.

Asaka, Y., Jugloff, D. G. M., Zhang, L., Eubanks, J. H., & Fitzsimonds, R. M. (2006). Hippocampal synaptic plasticity is impaired in the Mecp2-null mouse model of Rett syndrome. *Neurobiology of Disease, 21,* 217-227.

Ballas, N., Lioy, D. T., Grunseich, C., & Mandel, G. (2009). Non-cell autonomous influence of MeCP2-deficient glia on neuronal dendritic morphology. *Nat Neurosci, 12,* 311-317.

Barr, Murray Llewellyn, and J. A. Kiernan. The Human Nervous System: An Anatomical Viewpoint. Philadelphia: Lippincott, 1993. Print.

Bandeira, F., Lent, R., & Herculano-Houzel, S. (2009). Changing numbers of neuronal and non-neuronal cells underlie postnatal brain growth in the rat. *Proc Natl Acad Sci U.S.A, 106,* 14108-14113.

Battaglia, F. P., G. Borensztajn and R. Bod (2012). "Structured cognition and neural systems: from rats to language." Neurosci Biobehav Rev 36(7): 1626-1639.

Bauman, M. L., T. L. Kemper and D. M. Arin (1995). "Microscopic observations of the brain in Rett syndrome." Neuropediatrics 26(2): 105-108.

Bauman, M. L., T. L. Kemper and D. M. Arin (1995). "Pervasive neuroanatomic abnormalities of the brain in three cases of Rett's syndrome." Neurology 45(8): 1581-1586.

Belichenko, P. V., Hagberg, B., & Dahlstrom, A. (1997). Morphological study of neocortical areas in Rett syndrome. *Acta Neuropathol., 93,* 50-61.

Belichenko, P. V., E. E. Wright, N. P. Belichenko, E. Masliah, H. H. Li, W. C. Mobley and U. Francke (2009). "Widespread changes in dendritic and axonal morphology in Mecp2-mutant mouse models of Rett syndrome: evidence for disruption of neuronal networks." J Comp Neurol **514**(3): 240-258.

Bushong, E. A., Martone, M. E., & Ellisman, M. H. (2004). Maturation of astrocyte morphology and the establishment of astrocyte domains during postnatal hippocampal development. *Int.J.Dev.Neurosci., 22,* 73-86.

Chahrour, M., Jung, S. Y., Shaw, C., Zhou, X., Wong, S. T. C., Qin, J. et al. (2008). MeCP2, a Key Contributor to Neurological Disease, Activates and Represses Transcription. *Science, 320,* 1224-1229.

Chang, Q., Khare, G., Dani, V., Nelson, S., & Jaenisch, R. (2006). The disease progression of Mecp2 mutant mice is affected by the level of BDNF expression. *Neuron, 49,* 341-348.

Cuddapah, V. A., Pillai, R. B., Shekar, K. V., Lane, J. B., Motil, K. J., Skinner, S. A. et al. (2014). Methyl-CpG-binding protein 2 (MECP2) mutation type is associated with disease severity in Rett syndrome. *J.Med.Genet., 51,* 152-158.

Cuddapah, V. A., Nwaobi, S. E., Olsen, M.L., (2015). MeCP2 in the regulation of neural activity: Rett syndrome pathophysiological perspectives. Degenerative Neurological and Neuromuscular Disease 5, 103-116.

D'Cruz, J. A., Wu, C., Zahid, T., El-Hayek, Y., Zhang, L., & Eubanks, J. H. (2010). Alterations of cortical and hippocampal EEG activity in MeCP2-deficient mice. *Neurobiol.Dis., 38,* 8-16.

Dani, V. S., Chang, Q., Maffei, A., Turrigiano, G. G., Jaenisch, R., & Nelson, S. B. (2005). Reduced cortical activity due to a shift in the balance between excitation and inhibition in a mouse model of Rett syndrome. *Proc.Natl.Acad.Sci.U.S.A, 102,* 12560-12565.

Durand, S., Patrizi, A., Quast, K. B., Hachigian, L., Pavlyuk, R., Saxena, A. et al. (2012). NMDA receptor regulation prevents regression of visual cortical function in the absence of Mecp2. *Neuron, 76,* 1078-1090.

Ferreira, T. A., L. L. Iacono and C. T. Gross (2010). "Serotonin receptor 1A modulates actin dynamics and restricts dendritic growth in hippocampal neurons." Eur J Neurosci **32**(1): 18-26.

Freeman, M. R. (2010). Specification and morphogenesis of astrocytes. *Science, 330,* 774-778.

Hagberg, B., Aicardi, J., Dias, K., & Ramos, O. (1983). A progressive syndrome of autism, dementia, ataxia, and loss of purposeful hand use in girls: Rett's syndrome: report of 35 cases. *Ann.Neurol., 14,* 471-479.

Hatada, I., Namihira, M., Morita, S., Kimura, M., Horii, T., & Nakashima, K. (2008). Astrocyte-specific genes are generally demethylated in neural precursor cells prior to astrocytic differentiation. *PLoS One., 3,* e3189.

Jellinger, K., Armstrong, D., Zoghbi, H. Y., & Percy, A. K. (1988). Neuropathology of Rett syndrome. *Acta Neuropathol., 76,* 142-158.

Jentarra, G. M., S. L. Olfers, S. G. Rice, N. Srivastava, G. E. Homanics, M. Blue, S. Naidu and V. Narayanan (2010). "Abnormalities of cell packing density and dendritic complexity in the MeCP2 A140V mouse model of Rett syndrome/X-linked mental retardation." BMC Neurosci **11**: 19.

Kishi, N. & Macklis, J. D. (2004). MECP2 is progressively expressed in post-migratory neurons and is involved in neuronal maturation rather than cell fate decisions. Molecular and Cellular Neuroscience, 27, 306-321.

Kutzing, M. K., C. G. Langhammer, V. Luo, H. Lakdawala and B. L. Firestein (2010). "Automated Sholl analysis of digitized neuronal morphology at multiple scales." J Vis Exp(45).

Laurvick, C. L., de, K. N., Bower, C., Christodoulou, J., Ravine, D., Ellaway, C. et al. (2006). Rett syndrome in Australia: a review of the epidemiology. *J Pediatr., 148,* 347-352.

Lioy, D. T., Garg, S. K., Monaghan, C. E., Raber, J., Foust, K. D., Kaspar, B. K. et al. (2011). A role for glia in the progression of Rett's syndrome. *Nature, 475,* 497-500.

Lovatt, D., U. Sonnewald, H. S. Waagepetersen, A. Schousboe, W. He, J. H. Lin, X. Han, T. Takano, S. Wang, F. J. Sim, S. A. Goldman and M. Nedergaard (2007). "The transcriptome and metabolic gene signature of protoplasmic astrocytes in the adult murine cortex." J.Neurosci. **27**(45): 12255-12266.

Maezawa, I., Swanberg, S., Harvey, D., LaSalle, J. M., & Jin, L. W. (2009). Rett Syndrome Astrocytes Are Abnormal and Spread MeCP2 Deficiency through Gap Junctions. *Journal of Neuroscience, 29,* 5051-5061.

Martinowich, K., Hattori, D., Wu, H., Fouse, S., He, F., Hu, Y. et al. (2003). DNA methylation-related chromatin remodeling in activity-dependent BDNF gene regulation. *Science, 302,* 890-893.

McLeod, F., Ganley, R., Williams, L., Selfridge, J., Bird, A., & Cobb, S. R. (2013). Reduced seizure threshold and altered network oscillatory properties in a mouse model of Rett syndrome. *Neuroscience, 231,* 195-205.

Neul, J. L., Fang, P., Barrish, J., Lane, J., Caeg, E. B., Smith, E. O. et al. (2008). Specific mutations in methyl-CpG-binding protein 2 confer different severity in Rett syndrome. *Neurology, 70,* 1313-1321.

Neul, J. L., Kaufmann, W. E., Glaze, D. G., Christodoulou, J., Clarke, A. J., Bahi-Buisson, N. et al. (2010). Rett syndrome: revised diagnostic criteria and nomenclature. *Ann.Neurol., 68,* 944-950.

Nguyen, M. V., Du, F., Felice, C. A., Shan, X., Nigam, A., Mandel, G. et al. (2012). MeCP2 is critical for maintaining mature neuronal networks and global brain anatomy during late stages of postnatal brain development and in the mature adult brain. *Journal of Neuroscience, 32,* 10021-10034.

Oberheim, N. A., Wang, X., Goldman, S., & Nedergaard, M. (2006). Astrocytic complexity distinguishes the human brain. *Trends Neurosci., 29,* 547-553.

Panksepp, J. (1981). "The ontogeny of play in rats." Dev Psychobiol **14**(4): 327-332.

Patterson, K. C., V. E. Hawkins, K. M. Arps, D. K. Mulkey and M. L. Olsen (2016). "MeCP2 Deficiency Results in Robust Rett-like Behavioral and Motor Deficits in Male and Female Rats." Hum Mol Genet.

Pellis, S. M. and M. McKenna (1995). "What do rats find rewarding in play fighting?--an analysis using drug-induced non-playful partners." Behav Brain Res **68**(1): 65-73.

Pellis, S. M. and V. C. Pellis (1997). "The prejuvenile onset of play fighting in laboratory rats (Rattus norvegicus)." Dev Psychobiol **31**(3): 193-205.

Pellis, S. M. and V. C. Pellis (1998). "Play fighting of rats in comparative perspective: a schema for neurobehavioral analyses." Neurosci Biobehav Rev **23**(1): 87-101.

Purpura, D. P. (1974). "Dendritic spine "dysgenesis" and mental retardation." Science **186**(4169): 1126-1128.

Ronnett, G. V., D. Leopold, X. Cai, K. C. Hoffbuhr, L. Moses, E. P. Hoffman and S. Naidu (2003). "Olfactory biopsies demonstrate a defect in neuronal development in Rett's syndrome." Ann Neurol **54**(2): 206-218.

Schaevitz, L. R., N. B. Gomez, D. P. Zhen and J. E. Berger-Sweeney (2013). "MeCP2 R168X male and female mutant mice exhibit Rett-like behavioral deficits." Genes Brain Behav **12**(7): 732-740.

Sofroniew, M. V. & Vinters, H. V. (2010). Astrocytes: biology and pathology. *Acta Neuropathol., 119,* 7-35.

Thor, D. H. and W. R. Holloway, Jr. (1984). "Social play in juvenile rats: a decade of methodological and experimental research." Neurosci Biobehav Rev **8**(4): 455-464.

Tropea, D., Giacometti, E., Wilson, N. R., Beard, C., McCurry, C., Fu, D. D. et al. (2009). Partial reversal of Rett Syndrome-like symptoms in MeCP2 mutant mice. *Proc.Natl.Acad.Sci.U.S.A, 106,* 2029-2034.

Urcelay, G. P. and R. R. Miller (2010). "On the generality and limits of abstraction in rats and humans." Anim Cogn **13**(1): 21-32.

Zachariah, R. M. & Rastegar, M. (2012). Linking epigenetics to human disease and Rett syndrome: the emerging novel and challenging concepts in MeCP2 research. *Neural Plast., 2012,* 415825.

Zhang, L., He, J., Jugloff, D. G. M., & Eubanks, J. H. (2008). The MeCP2-null mouse hippocampus displays altered basal inhibitory rhythms and is prone to hyperexcitability. *Hippocampus, 18,* 294-309.

APPENDIX A

IACUC APPROVAL FORM

THE UNIVERSITY OF ALABAMA AT BIRMINGHAM

Institutional Animal Care and Use Committee (IACUC)

MEMORANDUM

DATE: June 6, 2014

TO: MICHELLE L OLSEN, D.Sc.
MCLM-958A
(205) 975-2715

FROM:

Robert A. Kesterson, Ph.D., Chair
Institutional Animal Care and Use Committee (IACUC)

SUBJECT: **NOTICE OF APPROVAL - Please forward this notice to the appropriate granting agency.**

The following application was approved by the University of Alabama at Birmingham Institutional Animal Care and Use Committee (IACUC) on June 6, 2014.

Title: Altered K+ Ion and Glutamate Homeostasis in Rett Syndrome
Sponsor: Rett Syndrome Research Foundation

This institution has an Animal Welfare Assurance on file with the Office of Laboratory Animal Welfare (OLAW), is registered as a Research Facility with the USDA, and is accredited by the Association for Assessment and Accreditation of Laboratory Animal Care International (AAALAC).

Institutional Animal Care and Use Committee (IACUC)
CH19 Suite 403
933 19th Street South
(205) 934-7692
FAX (205) 934-1188

Mailing Address:
CH19 Suite 403
1530 3rd Ave S
Birmingham, AL 35294-0019

Michelle L Olsen

From: Office of IACUC UAB <iacuc@uab.edu>
Sent: Wednesday, September 09, 2015 9:46 AM
To: Michelle L Olsen
Cc: Leanne M Holt
Subject: IACUC Approval for Modification of Animal Protocol Number (APN): IACUC-09409

DO NOT Reply or Reply All to this email!

Protocol PI: Michelle L Olsen
Title: Altered K+ Ion and Glutamate Homeostasis in Rett Syndrome
Sponsor: Rett Syndrome Research Foundation
Animal Project Number (APN): IACUC-09409

On 9/9/2015, the UAB Institutional Animal Care and Use Committee (IACUC) approved the proposed modification: Personnel: Kenneth Taylor Holt. The sponsor for this project may require notification of modification(s) approved by the IACUC, but not included in the original grant proposal/experimental plan; please inform the sponsor if necessary.

Animal use must be renewed annually. Approval from the IACUC must be obtained before implementing any changes or modifications in the approved animal use. Refer to APN IACUC-09409 when ordering animals or in any correspondence with the IACUC or Animal Resources Program (ARP) offices regarding this study. If you have concerns or questions regarding this notice, please call the IACUC office at (205) 934-7692.

IACUC Office
University of Alabama at Birmingham
CH19 Suite 403
933 19th Street South
Birmingham, Alabama 35294-2041
Voice: 204-934-7692
FAX: 204-934-1188
www.uab.edu/iacuc

1